Forschungszentrum Karlsruhe
Technik und Umwelt
Wissenschaftliche Berichte
FZKA 5802

T-stress in Edge-cracked Specimens

T. Fett
Institut für Materialforschung

Juli 1996

FORSCHUNGSZENTRUM KARLSRUHE

Technik und Umwelt

Wissenschaftliche Berichte

FZKA 5802

T-stress in edge-cracked specimens

T. Fett

Institut für Materialforschung

Forschungszentrum Karlsruhe GmbH, Karlsruhe

1996

Forschungszentrum Karlsruhe GmbH
Postfach 3640, 76021 Karlsruhe

ISSN 0947-8620

Abstract

The first regular stress term of the crack-tip stress field, the so-called T-stress, has an influence on the fracture behaviour of cracked components. Whilst for the singular stress term - represented by the stress intensity factor - handbook solutions are available, there is a lack of T-stress data.
In this report some solutions are summarised for edge cracks in rectangular plates or bars and in circular discs. As special loadings the cases of pure tension, bending, thermal stresses, and single forces are considered.

Der Konstant-Spannungsterm in Platten mit Außenrissen

Zusammenfassung

Der erste reguläre Spannungsterm des Rißspitzen-Spannungsfelds - der sogenannte T-stress-Term - besitzt neben dem dominierenden singulären Spannungsterm einen Einfluß auf das Bruchverhalten von rißbehafteten Bauteilen. Während für den Spannungsintensitätsfaktor, der das singuläre Spannungsfeld an einer Rißspitze charakterisiert, Handbuch-Lösungen verfügbar sind, herrscht Mangel an entsprechenden Daten für den Konstantspannungsterm T.
Im vorliegenden Bericht werden einige Lösungen für seitliche, durchgehende Risse in Platten bzw. Balken sowie in Kreisscheiben zusammengestellt. Als Belastungen werden Zug, Biegung, Thermospannungen und Einzelkräfte betrachtet.

Contents

1. Introduction **3**

2. T-stress term **5**

2.1 The Airy stress function 5

2.2 Determination of the coefficients A_0 and A_0^* 8

3. Green's function for T-stress **9**

3.1 Representation of T-stresses by a Green's function 9

3.2 Set-up for the Green's function and application 11

3.2.1 Approximation of the Green's function by direct adjustment to reference loading cases 12

4. Edge-cracked rectangular plate **15**

4.1 Influence of plate length 15

4.2 Long edge-cracked plate 18

4.3 Rectangular plate with thermal stresses 19

5. DCB-specimen **21**

6. Edge-cracked circular disc **23**

6.1 Circumferentially loaded disc 23

6.2 Diametrically loaded disc 24

6.3 Disc with thermal stresses 26

7. Cracks ahead of notches 31

8. Array of deep edge cracks 37

9. References 41

1. Introduction

In fracture mechanics most interest is focussed on stress intensity factors, which describe the singular stress field ahead of a crack tip and govern fracture of a specimen when a critical stress intensity factor is reached. Nevertheless, there is experimental evidence (e.g. [1]-[3]) that also the constant stress contributions acting over a longer distance from the crack tip may affect fracture mechanics properties. Apart from the singular stress term, the most important one is the so-called T-stress term which describes a constant stress parallel to crack direction.
Different methods were applied in the past to compute the T-stress term for fracture mechanics standard test specimens. Regarding one-dimendional cracks, Leevers and Radon [4] made a numerical analysis based on a variational method. Kfouri [5] applied an Eshelby-technique. Sham [6],[7] developed a second-order weight function based on a work-conjugate integral and evaluated it for the SEN specimen using the FE-method. In [8] a Green's function for T-stresses was determined on the basis of Boundary-Collocation results. Direct adjustment of the Green's function to reference T-stress solutions was made (see also [9]). Wang and Parks [10] extended the T-stress evaluation to two-dimensional surface cracks and used the line-spring method.
The aim of this report is to collect T-stress solutions for edge-cracked specimens under different loadings.

2. T-stress term

2.1 The Airy stress function

The total stress state in a cracked body is known if the Airy stress function Φ is available. The stress function can be obtained by solving the equation of compatibility

$$\Delta\Delta\Phi = 0 \tag{1}$$

For a cracked body a series representation for Φ was given by Williams [11]. Its symmetric part can be written

$$\Phi = \sigma^* W^2 \sum_{n=0}^{\infty} (r/W)^{n+3/2} A_n \left[\cos(n+3/2)\varphi - \frac{n+3/2}{n-1/2} \cos(n-1/2)\varphi \right]$$
$$+ \sigma^* W^2 \sum_{n=0}^{\infty} (r/W)^{n+2} A_n^* [\cos(n+2)\varphi - \cos n\varphi] \tag{2}$$

with the characteristic stress σ^* which may be the remote tensile stress in tensile tests or the outer fibre tensile stress in bending. The geometrical data are explained in fig.1. From the stress function the stress components can be computed by

$$\sigma_r = \frac{1}{r}\frac{\partial\Phi}{\partial r} + \frac{1}{r^2}\frac{\partial^2\Phi}{\partial\varphi^2}$$

$$\sigma_\varphi = \frac{\partial^2\Phi}{\partial r^2} \tag{3}$$

$$\tau_{r\varphi} = \frac{1}{r^2}\frac{\partial\Phi}{\partial\varphi} - \frac{1}{r}\frac{\partial^2\Phi}{\partial r\partial\varphi}$$

where r and φ are polar coordinates with the pole in the crack tip. One obtains

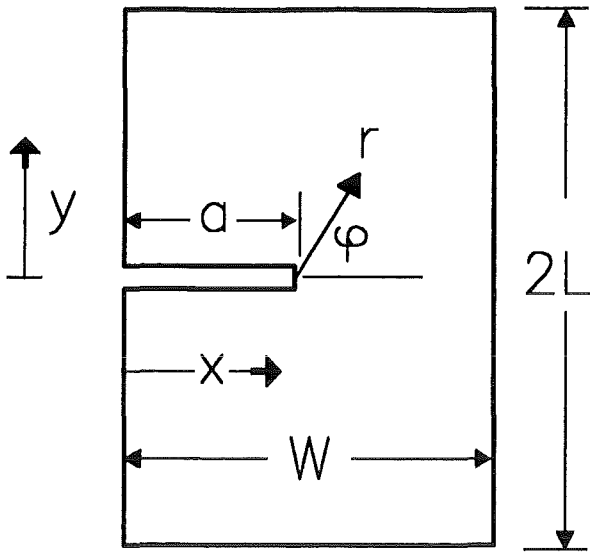

Figure 1. . Crack in a component; definition of polar coordinates.

$$\frac{\sigma_r}{\sigma^*} = \sum_{n=0}^{\infty} A_n \left(\frac{r}{W}\right)^{n-1/2} (n+3/2)\left[\frac{n^2-2n-5/4}{n-1/2}\cos(n-1/2)\varphi - (n+1/2)\cos(n+3/2)\varphi\right] + \sum_{n=0}^{\infty} A_n^* \left(\frac{r}{W}\right)^{n}\left[(n^2-n-2)\cos n\varphi - (n+2)(n+1)\cos(n+2)\varphi\right] \tag{4}$$

$$\frac{\sigma_\varphi}{\sigma^*} = \sum_{n=0}^{\infty} A_n \left(\frac{r}{W}\right)^{n-1/2} (n+3/2)(n+1/2)\left[\cos(n+3/2)\varphi - \frac{n+3/2}{n-1/2}\cos(n-1/2)\varphi\right] + \sum_{n=0}^{\infty} A_n^* \left(\frac{r}{W}\right)^{n}(n+2)(n+1)\left[\cos(n+2)\varphi - \cos n\varphi\right] \tag{5}$$

$$\frac{\tau_{r\varphi}}{\sigma^*} = \sum_{n=0}^{\infty} A_n \left(\frac{r}{W}\right)^{n-1/2} (n+3/2)(n+1/2)\left[\sin(n+3/2)\varphi - \sin(n-1/2)\varphi\right] + \sum_{n=0}^{\infty} A_n^* \left(\frac{r}{W}\right)^{n}(n+1)\left[(n+2)\sin(n+2)\varphi - n\sin n\varphi\right] \tag{6}$$

The unknown coefficients A_n and A^* have to be determined for the special specimen/crack-geometry and the chosen loading mode. Especially for the stress component σ_x ahead of the crack ($\varphi = 0$), eq.(4) reads

$$\sigma_x/\sigma^* = -\sum_{n=0}^{\infty} 2A_n (r/W)^{n-1/2}\left(n+\frac{3}{2}\right)\frac{2n+1}{2n-1} - \sum_{n=0}^{\infty} 4A_n^*(r/W)^n (n-1) \tag{7}$$

In fracture mechanics most interest is focussed on the stress intensity factor characterising the singular stress field ahead of a crack tip. The related stress singularity is responsible mainly for the failure of cracked components. The stress intensity factor K_I is related to coefficient A_0 by

$$K_I = \sigma^* F \sqrt{\pi a} \quad , \quad F = \sqrt{18/\alpha}\, A_0 \; , \quad \alpha = a/W \tag{8}$$

with the geometric function F. As Larsson and Carlsson [1] showed very early, there is experimental evidence that also the constant stress contributions acting over a longer distance from the crack tip may affect fracture mechanics properties. The related coefficient A_0^* leads to the constant stress term. If no x-stress component is present in the uncracked structure, the total x-stress is given by the so-called T-stress T

$$\sigma_x = T = -4\sigma^* A_0^* \tag{9}$$

Following a suggestion by Leevers and Radon [4], the T-stress can be dimensionless expressed by the "stress biaxiality ratio" β

$$\beta = \frac{T\sqrt{\pi a}}{K_I} \tag{10}$$

or written in terms of coefficients A_0, A_0^* as

$$\beta = \frac{T}{\sigma^* F} = -\frac{4}{\sqrt{18}}\sqrt{\alpha}\,\frac{A_0^*}{A_0} \tag{11}$$

Introducing the normalised coefficients

$$B_0 = A_0 (1-\alpha)^{3/2}/\sqrt{\alpha} \tag{12}$$

$$B_0^* = A_0^* (1-\alpha)^2 \tag{13}$$

we find

$$\beta = \frac{T}{\sigma^* F} = -\frac{4}{\sqrt{18(1-\alpha)}}\,\frac{B_0^*}{B_0} \tag{14}$$

If in the uncracked component already an x-stress is present, the effective x-component of stresses at the crack tip ($x = a$) is given as the sum of the x-stress component in the uncracked structure $\sigma_{x,0}$ and the contribution due to the presence of the crack, the so-called T-stress term

$$\sigma_{x,\,eff} = T + \sigma_{x,0} \tag{15}$$

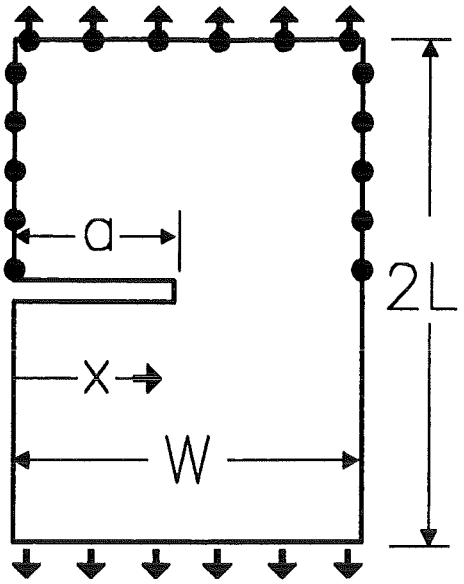

Figure 2. BCM. Edge-cracked plate under tensile loading with collocation points.

2.2 Determination of the coefficients A_0 and A_0^*

A simple possibility to determine the coefficients A_0 and A_0^* is the application of the Boundary Collocation Method (BCM). For practical application of eq.(2), which is used to determine A_0 and A_0^*, the infinite series must be truncated after the Nth term for which an adequate value must be chosen. The still unknown coefficients are determined by fitting the stresses to the specified boundary conditions at the surface. In case of the edge-cracked rectangular plate of width W and length $2L$ (fig.2) the stresses at the border are

$$\sigma_x = 0 \quad , \quad \tau_{xy} = 0 \quad \text{for} \quad x = 0 \tag{16}$$

$$\sigma_y = \sigma^* \quad , \quad \tau_{xy} = 0 \quad \text{for} \quad y = L \tag{17}$$

$$\sigma_x = 0 \quad , \quad \tau_{xy} = 0 \quad \text{for} \quad x = W \tag{18}$$

About 100-120 coefficients for eq.(2) were determined from 800 stress equations given at 400 nodes along the outer contour (symbolised by the circles in fig.2). For a selected number of (N+1) edge points the related stress components are computed, and we obtain a system of 2(N+1) equations with 2(N+1) unknowns whose solutions allow all 2(N+1) coefficients of eq.(2) to be determined.
The expenditure in terms of computation can be reduced by selection of a rather large number of edge points and by solving subsequently the then overdetermined system of equations using the least squares of deviations so that a set of "best" coefficients is obtained. The Harwell subroutine V02AD is used here to determine the best fit.

3. Green's function for T-stress

3.1 Representation of T-stresses by a Green's function

As a consequence of the principle of superposition for linear-elastic problems the T-stress term can be expressed by an integral (fig.3a)

$$T = \int_0^a t(x,a)\,\sigma(x)\,dx \tag{19}$$

where $t(x,a)$ is the Green's function for the T-stress, i.e. the T-value resulting for a pair of single unit forces. If we represent the single force P by a stress distribution

$$\sigma_y(x) = \frac{P}{B}\,\delta(x - x_0) \tag{20}$$

(see fig.3b) where δ is the Dirac δ-function and B is the thickness of the plate.

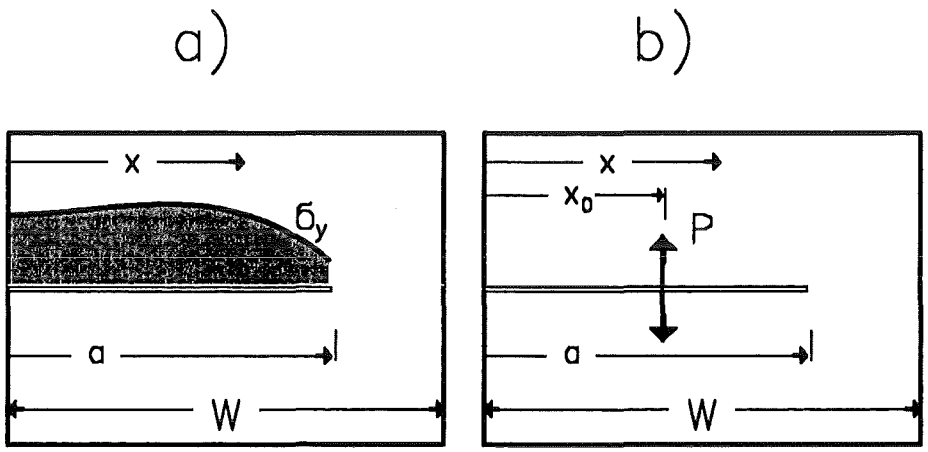

Figure 3. Green's function for T-stress. Edge-cracked plate: a) crack loaded by continuously distributed normal stresses, b) crack loaded with a single pair of forces.

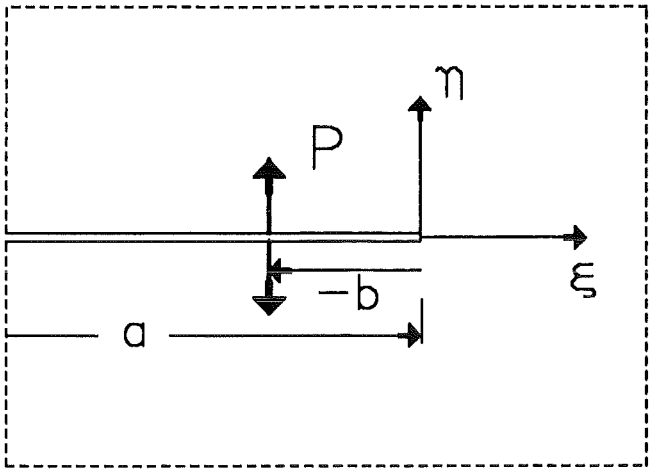

Figure 4. Green's function for T-stress. An infinite crack in an infinite body. Near-tip loading by a pair of single forces.

Introducing this stress into eq.(19) gives

$$T = \frac{P}{B}\int_0^a t(x,a)\,\delta(x - x_0)\,dx = \frac{P}{B}\,t(x_0,a) \tag{21}$$

i.e. the term $t(x_0,a)$ is the Green's function for the T-stress. In order to obtain information on the asymptotic behaviour of the weight or Green's function, we consider an infinitely long crack of length a in an infinite body which is loaded by a pair of forces acting at $\xi = -b$ (see fig.4). The related Westergaard stress function is ([12])

$$Z = \frac{P}{\pi}\frac{1}{z+b}\sqrt{\frac{b}{z}} \quad , \quad z = \xi + i\eta \tag{22}$$

The singular term results for $z \to 0$

$$Z_{sing} = \frac{P}{\pi}\frac{1}{\sqrt{b\,z}} \tag{23}$$

and the non-singular part follows as

$$Z_{reg} = Z - Z_{sing} = -\frac{P}{\pi}\frac{1}{z+b}\sqrt{\frac{z}{b}} \tag{24}$$

$$\sigma_{y,reg}\Big|_{y=0} = Re\{Z_{reg}\}\Big|_{y=0} \tag{25}$$

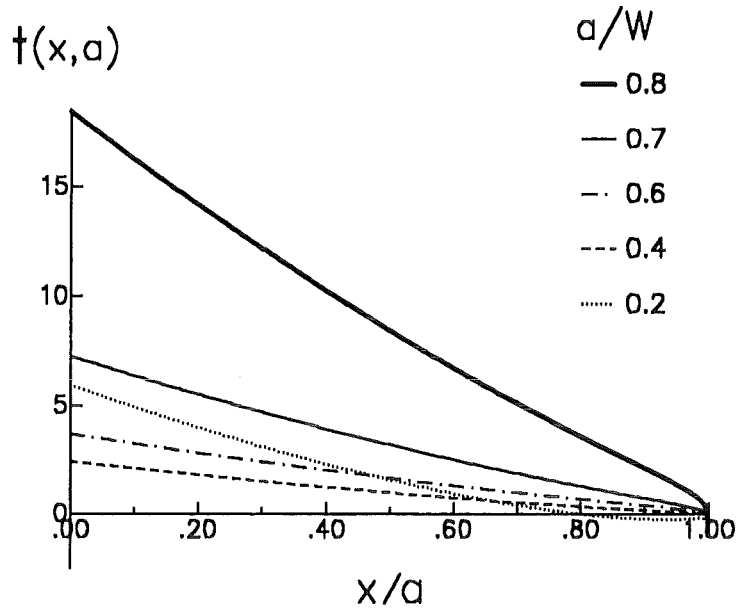

Figure 5. Green's function. Green's function for the T-stress term represented by the three-terms approximation, eqs.(29) and (33), for different relative crack sizes.

With the geometric data of fig.3 the asymptotic part then reads

$$t_0 = -\frac{1}{\pi}\frac{\sqrt{x'-a}}{(x'-x)\sqrt{a-x}} \quad , \quad x' > a \tag{26}$$

where x is the location where the normal stress σ_y acts on the crack faces and x' denotes the location where the σ_x-stress is computed. Integration of the singular term t_0 according to eq.(19) can be performed analytically for regular stress distributions, and the related T-stress term T_0 simply results as

$$T_0 = \lim_{x' \to a} \int_0^a t_0\, \sigma(x)\, dx = -\sigma\Big|_{x=a} \tag{27}$$

3.2 Set-up for the Green's function and application

It can be seen from eq.(26) that the dominating near-tip term of the Green's function is of the same order ($\propto 1/\sqrt{a-x}$) as the singular term in the weight function for stress intensity factors. Therefore, we will use the same type of set-up [9]

$$t = t_0 + \sum_{\nu=0}^{\infty} D_\nu (1 - x/a)^{\nu+1/2} \tag{28}$$

For the numerical evaluation we have to restrict the number of series terms. In the following considerations a three-term approximation will be used.

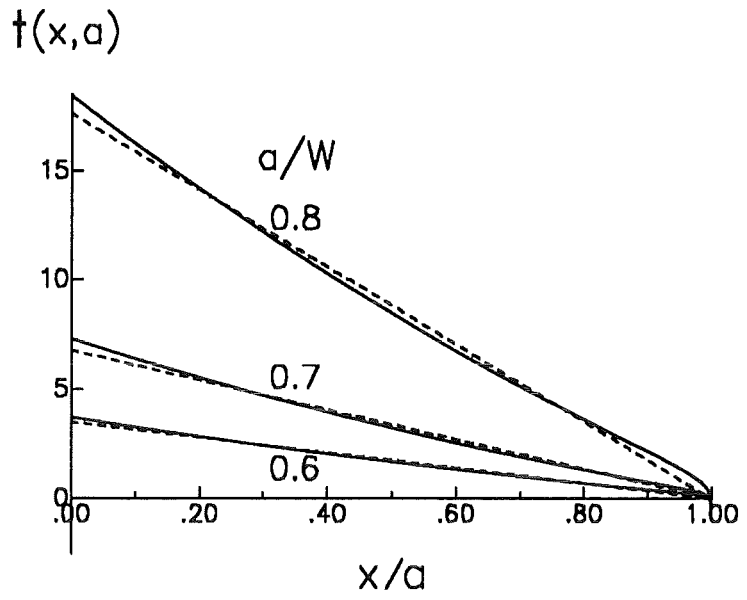

Figure 6. Green's function. Green's function for the T-stress term represented by the two-terms approximation (dashed lines), given by eqs.(34) and (36), compared with the three-terms approximation (solid curves) according to eqs.(29) and (32).

3.2.1 Approximation of the Green's function by direct adjustment to reference loading cases

The general treatment for the determination of the unknown coefficients from reference loading cases may be explained in case of a three-terms Green's function. According to eq.(28), we consider the approximation

$$t = t_0 + D_0\sqrt{1 - x/a} + D_1 (1 - x/a)^{3/2} \tag{29}$$

with t_0 defined by eq.(26). As the first reference loading case we use pure tension $\sigma = \sigma^*$. Introducing eq.(29) into eq.(19) gives, with $x/a = \rho$,

$$T_t/\sigma^* = -1 + D_0\, a\int_0^1 \sqrt{1 - \rho}\; d\rho + D_1\, a\int_0^1 (1 - \rho)^{3/2}\, d\rho \tag{30}$$

From the bending reference loading case it follows

$$\frac{T_b}{\sigma^*} = -1 + 2\alpha + D_0\, a\int_0^1 \sqrt{1 - \rho}\,(1 - 2\alpha\rho)d\rho + D_1\, a\int_0^1 (1 - \rho)^{3/2}\,(1 - 2\alpha\rho)d\rho \tag{31}$$

where T_t is the T-stress in tension and T_b is the T-stress in bending. The two relations, eqs.(30) and (31), provide the coefficients

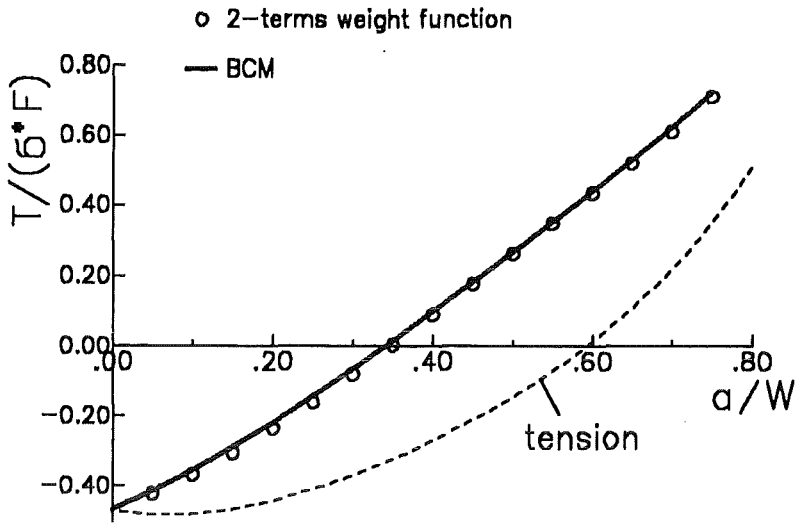

Figure 7. Biaxiality. Biaxiality ratio for bending computed from the T-stress approximation, eqs.(34) and (36) (circles); solid line: result for bending obtained with the Boundary Collocation Method [9]; dashed line: reference loading case tension.

$$D_0 = \frac{15}{16a}\left((7-4\alpha)\frac{T_t}{\sigma^*} - 7\frac{T_b}{\sigma^*} + 10\alpha\right)$$
$$D_1 = -\frac{35}{16a}\left((5-4\alpha)\frac{T_t}{\sigma^*} - 5\frac{T_b}{\sigma^*} + 6\alpha\right) \tag{32}$$

or after introducing eqs.(9), (39) and (41)

$$D_0 = \frac{15}{8W(1-\alpha)^2}\left(-0.3889 + 1.8706\alpha - 2.0012\alpha^2 - 1.0544\alpha^3 + 2.283\alpha^4 - 0.3932\alpha^5\right)$$
$$D_1 = -\frac{35}{8W(1-\alpha)^2}\left(-0.5487 + 2.1127\alpha - 2.1180\alpha^2 - 1.1845\alpha^3 + 2.0864\alpha^4 - 0.3932\alpha^5\right) \tag{33}$$

The three-term Green's function, described by eqs.(29) and (33), is plotted in fig.5. The negative singular term dominates only for $x/a > 0.99$.
In order to make a rough estimate of the Green's function which allows simplest computations to be performed, we arbitrarily assume the terms with the exponents 1/2 and 3/2 to be replaced by one single term with the intermediate exponent 1. Under this condition the two-terms approximation reads

$$t = t_0 + C\,(1 - x/a) \tag{34}$$

Introducing this set-up into eq.(19) and taking into consideration eq.(9), we obtain the relation

$$T_t/\sigma_0 = \int_0^a t(x,a)\,dx = -1 + \frac{a}{2}C = -4A_0^* \tag{35}$$

which provides the coefficient

$$C = \frac{2}{a}(1 - 4A_0^*) \tag{36}$$

Based on the tensile solution, the T-stress for bending has been computed by

$$T_b = \int_0^a t(x,a)\,\sigma^* \left(1 - 2\frac{x}{W}\right) dx \tag{37}$$

where W is the width of the plate and σ^* is the outer fibre stress. The result is plotted as the biaxiality ratio $T_b/(F\sigma^*)$ and represented as circles in fig.7. The solution based on Boundary Collocation computations [9]is represented by the solid curve. The dashed curve represents the reference loading case (tension) from which the coefficient D_1 has been determined. Although a rough approximation has been applied in this case, the agreement is excellent.

4. Edge-cracked rectangular plate

4.1 Influence of plate length

Figure 8 shows an edge-cracked rectangular plate under constant tensile stress. BCM-computations provided the coefficients A_0 and A_0^* which are entered in tables 1 and 2 and figures 9 and 10 for several plate lengths. The coefficients are represented in a normalised form according to eqs.(12) and (13). The biaxiality ratio is shown in table 3 and fig.11.

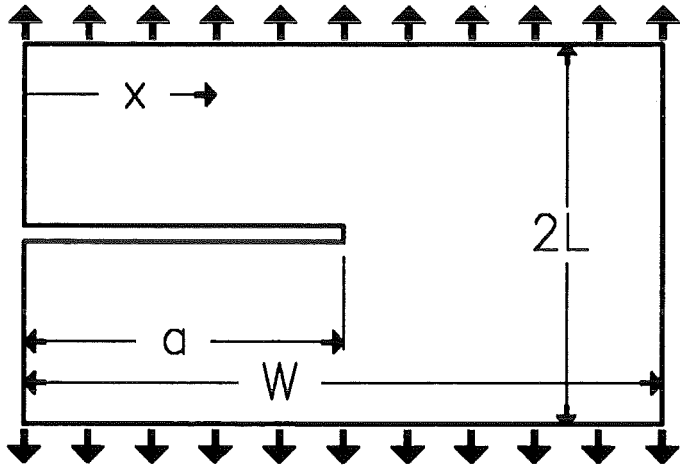

Figure 8. Edge-cracked plate. Short plate under tensile loading.

α	$L/W = 1.5$	0.75	0.50	0.40	0.30	0.25
0	0.2643	0.2643	0.2643	0.2643	0.2643	0.2643
0.1	0.2397	0.240	0.244	0.251	0.270	0.293
0.2	0.2315	0.232	0.251	0.274	0.321	0.362
0.3	0.230	0.231	0.255	0.286	0.351	0.406

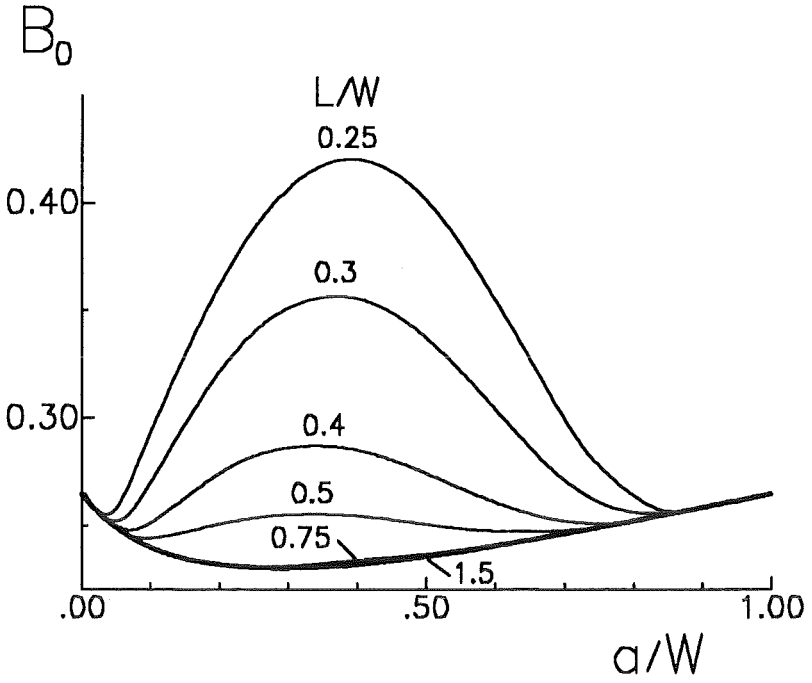

Figure 9. Coefficient A_0. Coefficient A_0 in representation $B_0 = A_0(1-\alpha)^{3/2}/\sqrt{\alpha}$.

0.4	0.231	0.234	0.255	0.285	0.355	0.420
0.5	0.235	0.237	0.251	0.275	0.337	0.401
0.6	0.240	0.241	0.247	0.261	0.304	0.355
0.7	0.246	0.246	0.248	0.252	0.271	0.299
0.8	0.252	0.252	0.252	0.253	0.256	0.264
0.9	0.258	0.258	0.258	0.258	0.258	0.269
1.0	0.2643	0.2643	0.2643	0.2643	0.2643	0.2643

Table 1. . Coefficients $B_0 = A_0\,(1-\alpha)^{3/2}/\sqrt{\alpha}$

α	$L/W = 1.5$	0.75	0.50	0.40	0.30	0.25
0	0.1315	0.1315	0.1315	0.1315	0.1315	0.1315
0.1	0.113	0.113	0.111	0.108	0.104	0.100
0.2	0.0936	0.0932	0.0835	0.0674	0.0211	-0.0335
0.3	0.0748	0.0706	0.0369	-0.0074	-0.1122	-0.2224
0.4	0.0521	0.0438	-0.0099	-0.0774	-0.2279	-0.3816
0.5	0.0264	0.0174	-0.0417	-0.1183	-0.2913	-0.4645
0.6	-0.0015	-0.0079	-0.0550	-0.1225	-0.2854	-0.4530

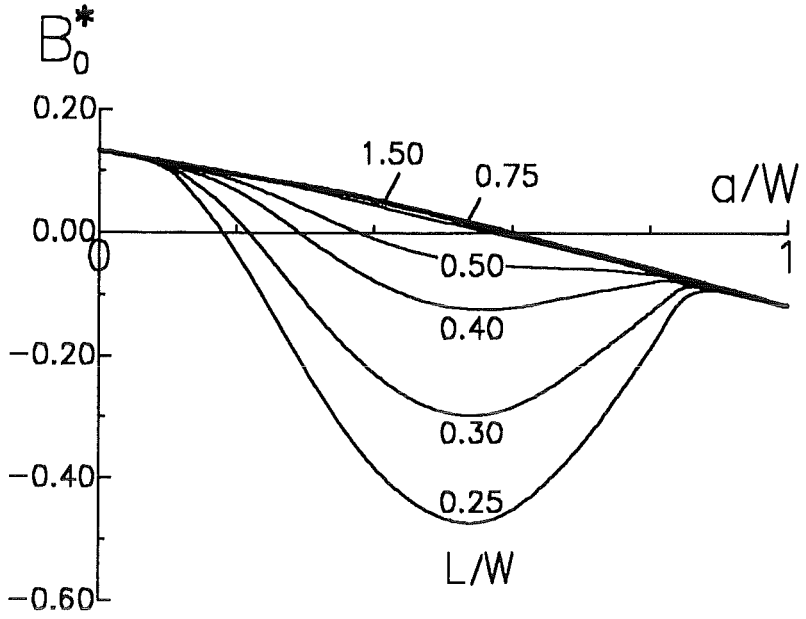

Figure 10. Coefficient A_{δ}^*. Coefficient A_{δ}^* in representation $B_{\delta}^* = A_{\delta}^*(1-\alpha)^2$.

0.7	-0.0306	-0.0334	-0.0585	-0.1009	-0.2172	-0.3468
0.8	-0.058	-0.060	-0.067	-0.081	-0.131	-0.190
0.9	-0.088	-0.089	-0.091	-0.093	-0.094	-0.095
1.0	-0.1185	-0.1185	-0.1185	-0.1185	-0.1185	-0.1185

Table 2. . Coefficients $B_{\delta}^* = A_{\delta}^*(1-\alpha)^2$

α	$L/W = 1.5$	0.75	0.50	0.40	0.30	0.25
0	-0.469	-0.469	-0.469	-0.469	-0.469	-0.469
0.1	-0.444	-0.444	-0.429	-0.406	-0.363	-0.322
0.2	-0.381	-0.379	-0.314	-0.232	-0.062	0.087
0.3	-0.307	-0.288	-0.137	0.024	0.302	0.516
0.4	-0.212	-0.177	0.037	0.256	0.605	0.856
0.5	-0.106	-0.069	0.157	0.406	0.814	-0.1091
0.6	0.006	0.031	0.209	0.443	0.885	1.204
0.7	0.117	0.128	0.223	0.377	0.755	1.092
0.8	0.217	0.226	0.252	0.305	0.480	0.678
0.9	0.321	0.325	0.332	0.341	0.343	0.346
1.0	0.4227	0.4227	0.4227	0.4227	0.4227	0.4227

Table 3. . Biaxiality ratio $\beta\sqrt{1-\alpha}$

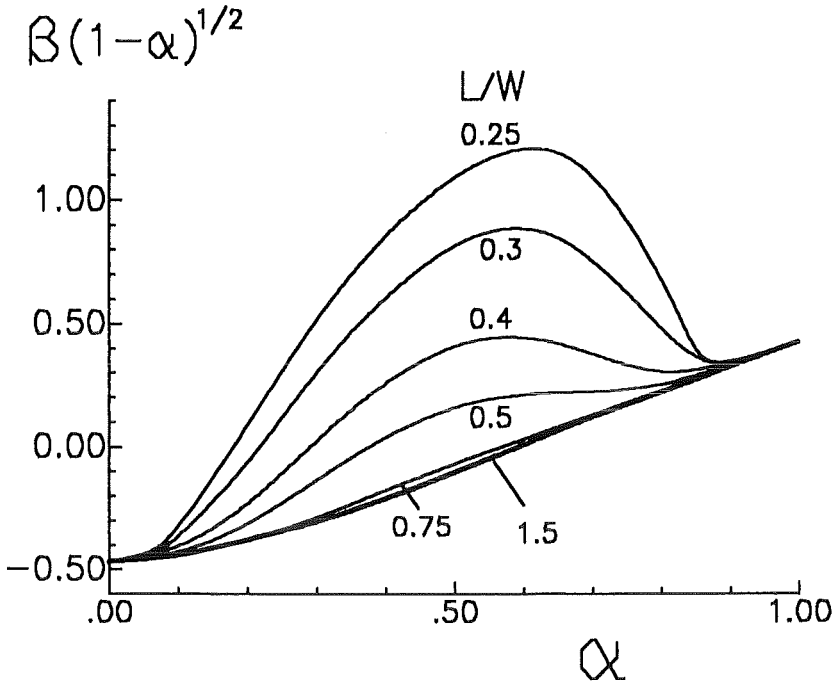

Figure 11. β. Biaxiality ratio in the form of $\beta\sqrt{1-\alpha}$

4.2 Long edge-cracked plate

The coefficients determined for the long edge-cracked plate were fitted and represented in polynomial form [9].

Tension

$$A_0 = \sqrt{\alpha}\ \frac{0.26434 - 0.39652\alpha + 1.5806\alpha^2 - 2.8451\alpha^3 + 2.5055\alpha^4 - 0.84445\alpha^5}{(1-\alpha)^{3/2}} \tag{38}$$

$$A_0^* = \frac{0.13149 - 0.16024\alpha - 0.051233\alpha^2 - 0.18874\alpha^3 + 0.19936\alpha^4 - 0.04915\alpha^5}{(1-\alpha)^2} \tag{39}$$

Bending

$$A_0 = \sqrt{\alpha}\ \frac{0.264345 - 0.55748\alpha + 0.8280\alpha^2 - 0.64818\alpha^3 + 0.20153\alpha^4}{(1-\alpha)^{3/2}} \tag{40}$$

$$A_0^* = \frac{0.13149 - 0.6203\alpha + 0.88823\alpha^2 - 0.65955\alpha^3 + 0.2319\alpha^4}{(1-\alpha)^2} \tag{41}$$

The biaxiality ratios for the long plate are given in fig.12.

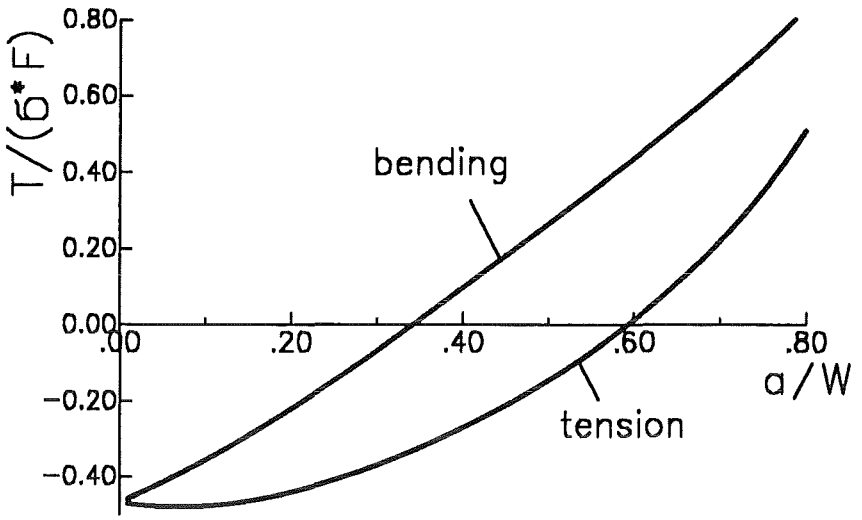

Figure 12. T-stress. Biaxiality ratio for the long edge-cracked plate

4.3 Rectangular plate with thermal stresses

A rectangular plate with a parabolically distributed temperature Θ

$$\Theta = 4\,\Theta_0\left(\frac{x}{W} - \left(\frac{x}{W}\right)^2\right) \tag{42}$$

is considered, wich causes a stress distribution

$$\sigma_y = \sigma^*\left(\frac{2}{3} - 4\,\frac{x}{W} + 4\,\frac{x^2}{W^2}\right) \qquad \sigma^* = \alpha_T\, T_0\, E \tag{43}$$

with E = Young's modulus and α_T = thermal expansion coefficient. The stress distribution is shown in the insert of fig.13. Introducing this stress distribution into eq.(19) yields the T-stress

$$T/\sigma^* = \frac{2}{3}(1-\alpha)^2(1-4A_0^*) + 4\alpha(1-\alpha) - \frac{2}{3} \tag{44}$$

with A_0^* taken from Table 2 or computed with eq.(39). The T-stress is plotted in fig.13. The corresponding stress intensity factor was calculated by

$$K_I = \int_0^a h(x,a)\,\sigma(x)\,dx \tag{45}$$

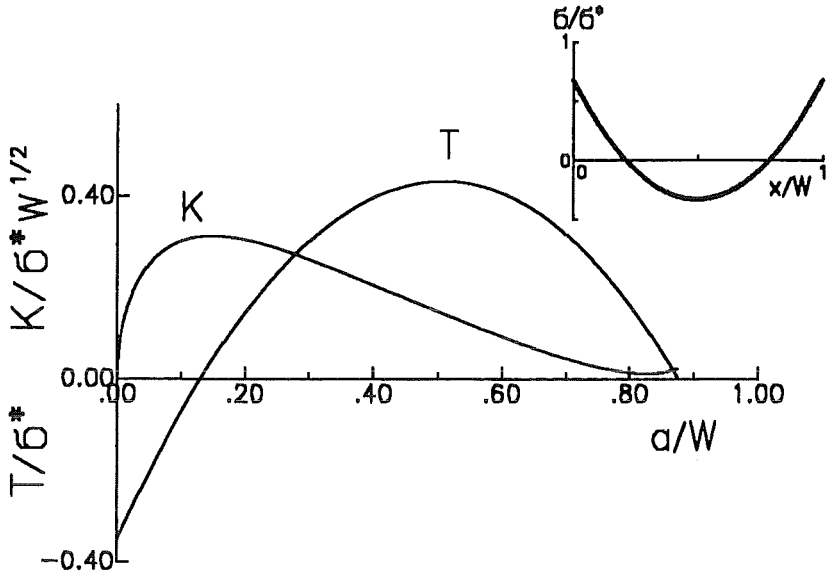

Figure 13. Thermal stress. Stress intensity factor and T-stress in a rectangular plate under thermal stress conditions. Insert: stress distribution according to eq.(43).

with the weight function h taken from [9]. The stress intensity factors have been entered additionally in fig.13. Finally, the biaxiality ratio β is represented in fig.14. Large positive biaxiality ratios are obvious for deep cracks. This is a consequence of the low stress intensity factors near $a/W = 0.8$.

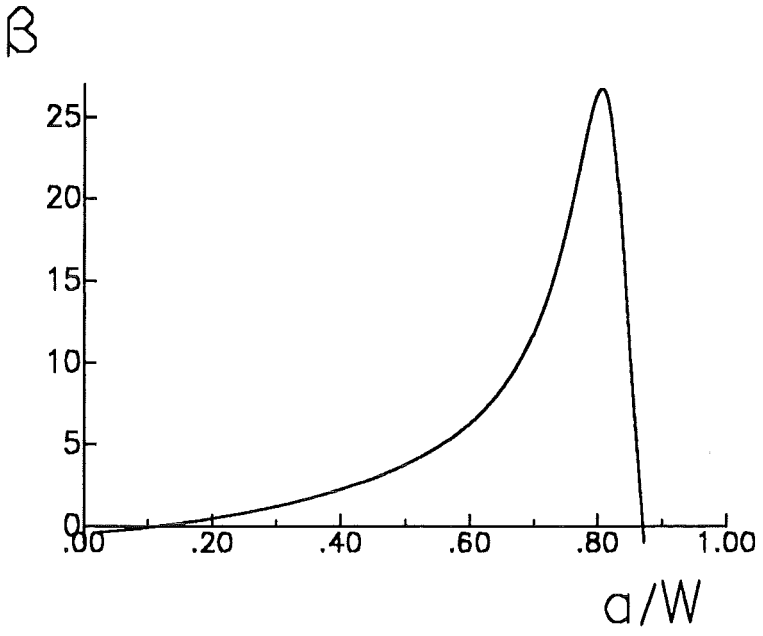

Figure 14. Thermal stress. Biaxiality ratio for thermal stresses given by eq.(43).

5. DCB-specimen

A Double-Cantilever-Beam(DCB) specimen is shown in fig.15. For the numerical considerations the width W was chosen to be $W/d > 3$. The stress intensity factor under constant tension as well as the T-stress term were determined by application of the Boundary Collocation Method. The β-values, obtained with BCM, are plotted in fig.16 as open symbols. Data from the literature (Leevers and Radon [4]) are entered as solid symbols. For $d/a < 0.5$ the β-ratio is found to be independent of a/W if $a/W \leq 0.55$. The averaging curve provides the relation

$$\frac{1}{\beta} \simeq 0.681 \frac{d}{a} + 0.0685 \tag{46}$$

which is represented in fig.16 by the solid line.

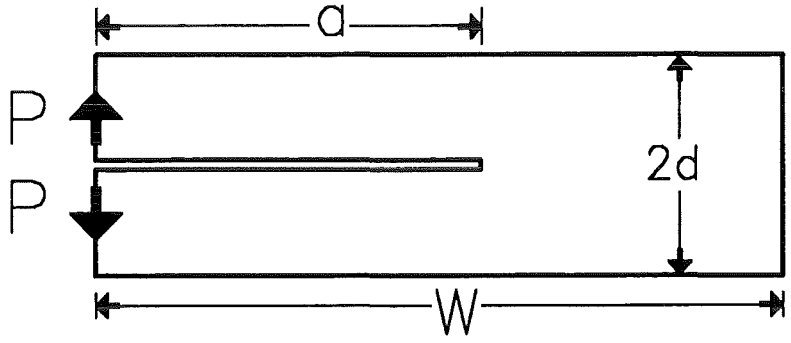

Figure 15. DCB-specimen. Geometrical data of a DCB-specimen.

The stress intensity factor solution is given by

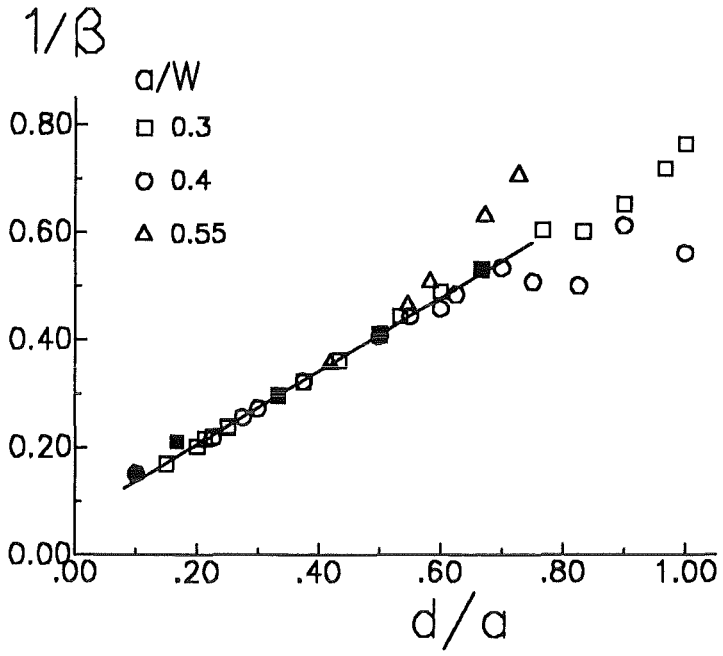

Figure 16. T-stress. Biaxiality ratio for the DCB-specimen as a function of d/a (computed for several ratios a/W). BCM-results: open symbols; Results of Leevers and Radon [4]: solid symbols; straight line: eq.(46).

$$K_I = \sqrt{\frac{12}{d}}\, P\left(\frac{a}{d} + 0.68\right) \tag{47}$$

The T-stress results from eqs.(46) and (47) as

$$T = \frac{\beta K_I}{\sqrt{\pi a}} \tag{48}$$

6. Edge-cracked circular disc

Edge-cracked circular discs are often used as fracture mechanics test specimens, especially in case of ceramic materials [13]-[15]. Figure 17 shows the geometric data.

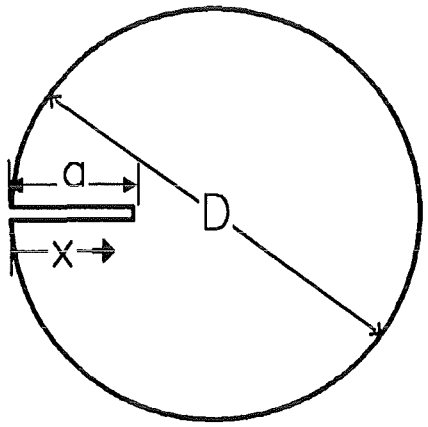

Figure 17. Circular disc. Geometric data of an edge-cracked disc.

6.1 Circumferentially loaded disc

A circular disc is loaded by constant normal tractions along the circumference

$$\sigma_n = const \ , \ \tau = 0 \tag{49}$$

In this case it holds [9]

$$A_0(1-\alpha)^{3/2}\,\alpha^{-1/2} \ = \ 0.2643452 = C_0 \tag{50}$$

$$A_0^*(1-\alpha)^2 \ = \ -0.11851 = C_0^* \tag{51}$$

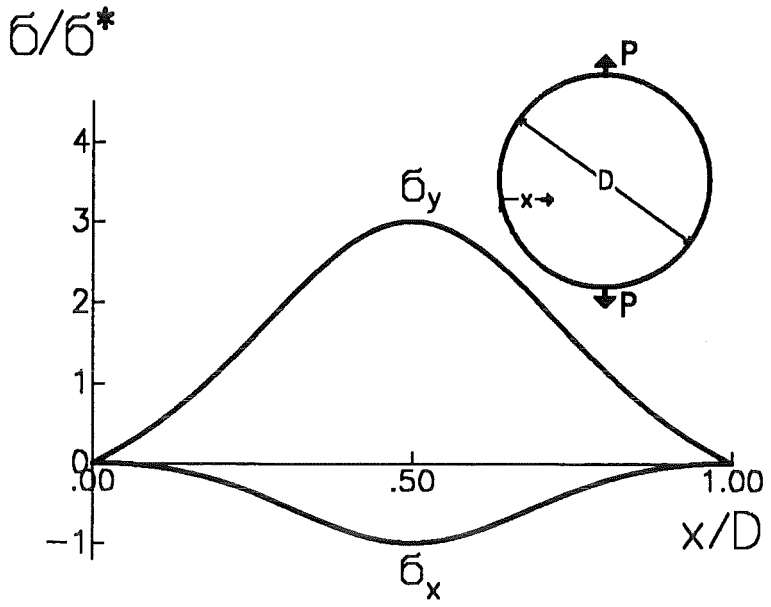

Figure 18. Circular disc. Stresses in a diametrically loaded circular disc (along the x-axis).

where the values C_0 and C_β are the coefficients of Wigglesworth's [16] expansion for the edge-cracked semi-infinite body.

6.2 Diametrically loaded disc

The Green's function method may be applied here to the diametrically loaded edge-cracked disc (see fig.18). In this case it holds [9]

$$A_0^* = -\frac{0.11851}{(1-\alpha)^2} + 1/4 \quad , \quad \alpha = a/D \tag{52}$$

As a consequence of eq.(19) it follows for the edge-cracked disc

$$T \simeq \frac{0.9481}{(1-\alpha)^2} \int_0^1 (1-\rho)\, \sigma_y(\rho)\, d\rho \; - \; \sigma_y\Big|_{x=a} \tag{53}$$

As an application we consider the disc of unit thickness which is diametrically loaded by a pair of forces P (see insert of fig.18). In this case the stresses are given by

$$\frac{\sigma_y}{\sigma^*} = \frac{4}{\left[1+(1-\xi)^2\right]^2} - 1 \quad , \quad \xi = x/R \, , \; R = D/2 \tag{54}$$

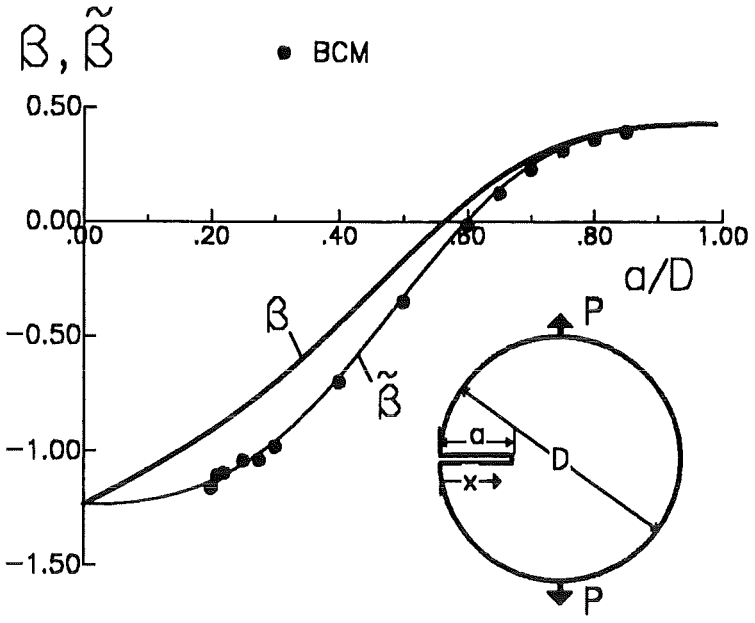

Figure 19. Circular disc. Biaxiality ratio for an edge-cracked circular disc diametrically loaded by a pair of forces; lines: eq.(56).

$$\frac{\sigma_x}{\sigma^*} = 1 - 4\frac{(1-\xi)^2}{\left[1+(1-\xi)^2\right]^2} \qquad , \sigma^* = \frac{P}{\pi R} \tag{55}$$

as illustrated in fig.18. Introducing σ_y in eq.(19) yields the T-stress term

$$T \simeq \frac{0.9481\sigma^*}{(1-\alpha)^2(a/R)^2}\left[4\left(1-\frac{a}{R}\right)arctan\left(1-\frac{a}{R}\right) + 2\frac{a}{R} - \left(\frac{a}{R}\right)^2 - \pi\left(1-\frac{a}{R}\right)\right] - \sigma_y\Big|_{x=a} \tag{56}$$

The stress intensity factor results from [17] as

$$K_I = \int_0^a h(x,a)\,\sigma_y\,dx \tag{57}$$

where h is the fracture mechanics weight function. In case of an edge-cracked disc a representation is given in [9], i.e.

$$h(x,a) = \sqrt{\frac{2}{\pi a}}\left[\frac{\rho}{\sqrt{1-\rho}} + D_0\sqrt{1-\rho} + D_1(1-\rho)^{3/2} + D_2(1-\rho)^{5/2}\right] \tag{58}$$

with the coefficients

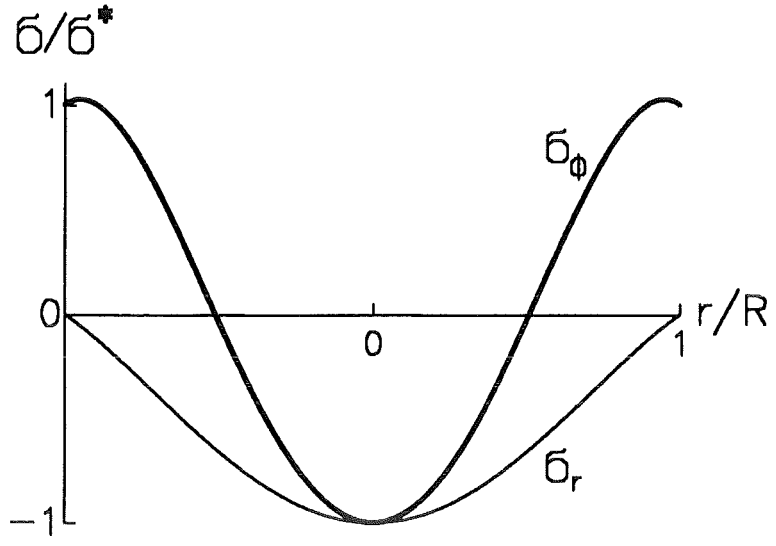

Figure 20. . Stress distributions in a thermally heated disc.

$$D_0 = (1.5721 + 2.4109\alpha - 0.8968\alpha^2 - 1.4311\alpha^3)/(1-\alpha)^{3/2}$$

$$D_1 = (0.4612 + 0.5972\alpha + 0.7466\alpha^2 + 2.2131\alpha^3)/(1-\alpha)^{3/2} \qquad (59)$$

$$D_2 = (-0.2537 + 0.4353\alpha - 0.2851\alpha^2 - 0.5853\alpha^3)/(1-\alpha)^{3/2}$$

By consideration of the total x-stress one can define an additional biaxiality ratio

$$\tilde{\beta} = \frac{-4\sigma^* A_0^* \sqrt{\pi a}}{K_I} = \left(\sigma_x\Big|_{x=a} + T\right) \frac{\sqrt{\pi a}}{K_I} \qquad (60)$$

The T-stress and the stress intensity factor result in the biaxiality ratios β and $\tilde{\beta}$ which are shown as curves in fig.19. In addition, the biaxiality ratios were directly determined with the Boundary Collocation Method (BCM) which provide the coefficient A_0^* for the situation of diametrical loading. The results - expressed by β - are entered as circles. An excellent agreement is obvious between the BCM results and those obtained from the Green's function representation. This is an indication of an adequate description of the Green's function by the set-up in eq.(34).

6.3 Disc with thermal stresses

In a thermally loaded circular disc the stresses in the absence of a crack consist of the circumferential stress component σ_φ and of the radial stress contribution σ_r. The two stress components can be computed from the temperature distribution $\Theta(r)$ with $r = D/2 - x$ (see e.g. [18])

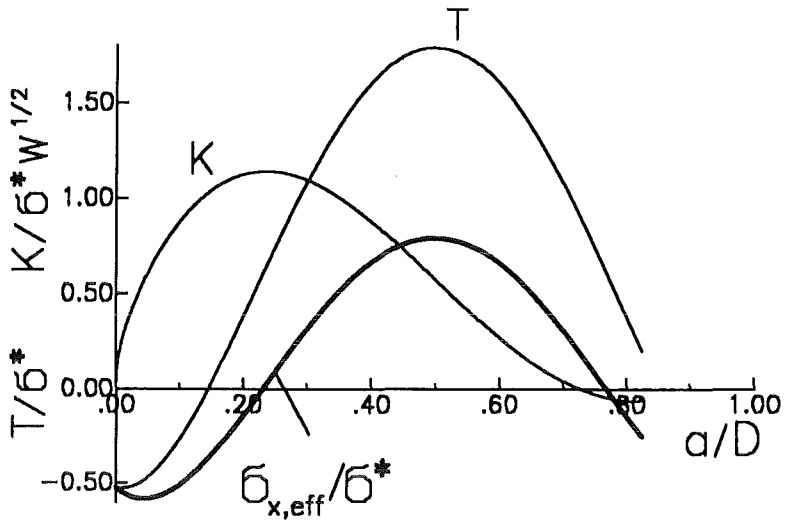

Figure 21. . Stress intensity factor, T-stress and total x-stress at the crack tip for thermal loading according to fig.20.

$$\sigma_r = \left(\frac{1}{R^2} \int_0^R \Theta\, r\, dr - \frac{1}{r^2} \int_0^r \Theta\, r\, dr \right) \tag{61}$$

$$\sigma_\varphi = \alpha E \left(\frac{1}{R^2} \int_0^R \Theta\, r\, dr + \frac{1}{r^2} \int_0^r \Theta\, r\, dr - \Theta \right) \tag{62}$$

In [14] the temperatures were found to be expressed by

$$\Theta(r) = \Theta_0 \left[1 + B_2 \left(\frac{r}{R} \right)^2 + B_4 \left(\frac{r}{R} \right)^4 \right] \tag{63}$$

with the maximum temperature Θ_0 occurring in the centre of the disc ($r = 0$). The related stresses are

$$\sigma_\varphi = \alpha E \Theta_0 \left[\frac{1}{4} B_2 + \frac{1}{6} B_4 - \frac{3}{4} B_2 \left(\frac{r}{R} \right)^2 - \frac{5}{6} B_4 \left(\frac{r}{R} \right)^4 \right] \tag{64}$$

$$\sigma_r = \alpha E \Theta_0 \left[\frac{1}{4} B_2 \left(1 - \frac{r^2}{R^2} \right) + \frac{1}{6} B_4 \left(1 - \frac{r^4}{R^4} \right) \right] \tag{65}$$

For a typical stress distribution in a thermally heated disc we can conclude from curves plotted in [14]

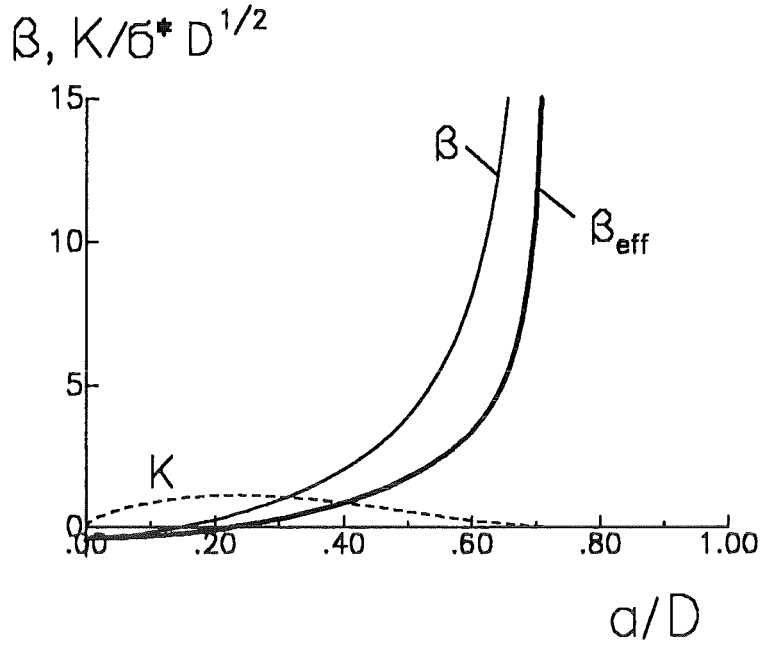

Figure 22. . Stress intensity factor, biaxiality ratio β, and effective biaxiality ratio β_{eff} defined by eq.(71).

$$\sigma_\varphi = -\sigma^*\left[1-\frac{9}{2}\left(\frac{r}{R}\right)^2+\frac{5}{2}\left(\frac{r}{R}\right)^4\right] \tag{66}$$

$$\sigma_r = -\sigma^*\left[1-\frac{3}{2}\left(\frac{r}{R}\right)^2+\frac{1}{2}\left(\frac{r}{R}\right)^4\right] \tag{67}$$

or

$$\sigma_\varphi = -\sigma^*\left[1-\frac{9}{2}\left(1-\frac{x}{R}\right)^2+\frac{5}{2}\left(1-\frac{x}{R}\right)^4\right] \tag{68}$$

$$\sigma_r = -\sigma^*\left[1-\frac{3}{2}\left(1-\frac{x}{R}\right)^2+\frac{1}{2}\left(1-\frac{x}{R}\right)^4\right] \tag{69}$$

where σ^* is the circumferential tensile stress at $r=R$. When eq.(19) is used, the thermal stresses result in the T-stress

$$T \simeq -0.15801\,\sigma^*\left[2\left(\frac{a}{R}\right)^2-4\frac{a}{R}-3\right]-\sigma_y\Big|_{x=a} \tag{70}$$

Equation (15) gives rise to definition of an effective biaxiality ratio

$$\beta_{eff} = \frac{\sqrt{\pi a}}{K_I}\,\sigma_{x,eff} \tag{71}$$

that includes the σ_x-stresses in the uncracked disc. The biaxiality ratio β and the effective biaxiality ratio β_{eff} were computed using the weight function for the edge-cracked disc. Figure 22 represents the biaxiality ratios for the thermally stressed edge-cracked disc. Very high values of the β-values occur for $a/D > 0.6$. The main reason is the very small stress intensity factor which disappears at approximately $a/D \simeq 0.7$.

7. Cracks ahead of notches

Special specimens contain narrow notches which are introduced in order to simulate a starter crack. This is for instance the case in fracture toughness experiments carried out on ceramics. A plate with a slender edge notch of depth a_0 is considered. A small crack of length ℓ is assumed to occur directly at the notch root with the radius R. The geometrical data are illustrated in fig.23.

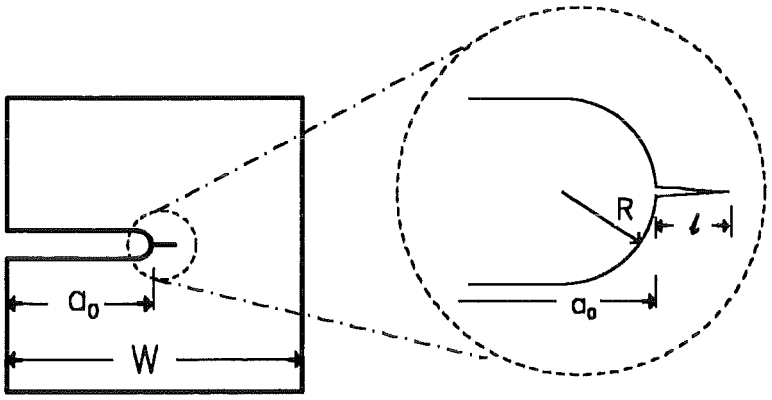

Figure 23. Circular notch. A small crack emanating from the root of a notch; geometric data.

In the absence of a crack the stresses near the notch root are given by

$$\sigma_y = \frac{2K(a_0)}{\sqrt{\pi(R+2\xi)}} \frac{R+\xi}{R+2\xi}$$
$$\sigma_x = \frac{2K(a_0)}{\sqrt{\pi(R+2\xi)}} \frac{\xi}{R+2\xi} \qquad (72)$$

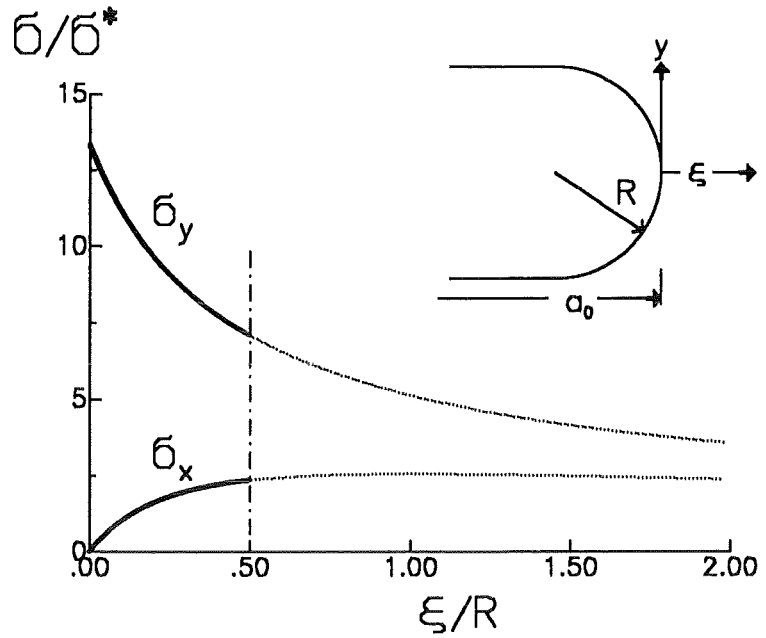

Figure 24. Notch stress. Stresses ahead of a slender notch computed according to Creager and Paris [19] for $a_0/W = 0.5$ and $R/W = 0.025$.

(for ξ see fig.24) as shown by Creager and Paris [19]. The quantity $K(a_0)$ is the stress intensity factor of a crack with the same length a_0 as the notch under identical external load

$$K(a_0) = \sigma^* F(a_0)\sqrt{\pi a_0} \tag{73}$$

with the characteristic stress σ^* and the geometric function F. The stresses resulting from eq.(72) are plotted in fig.24. The solid parts of the curves represent the region $(0 \leq \xi < R/2)$ where higher order terms are negligible. A small crack of length ℓ is considered which emanates from the notch root (see fig.23). Under externally applied load the coefficients of the stress function were calculated. The coefficient A_0 is related to the stress intensity factor K_I by

$$K_I = \sigma^* F(\ell)\sqrt{\pi\ell} \quad , \quad F(\ell) = \sqrt{18W/\ell}\, A_0 \tag{74}$$

with the geometric function F. If we *define* here the T-stress as the <u>total</u> x-stress resulting from the contribution of the notch in the absence of the crack <u>and</u> from the contribution of the crack, we have

$$\sigma_x = T = -4\sigma^* A_0^* \tag{75}$$

Boundary Collocation computations were performed and the results are plotted for bending in fig.25. In this case the reference stress is the outer fibre bending stress $\sigma^* = \sigma_b$ with

$$\sigma_b = \frac{6M}{W^2 B} \tag{76}$$

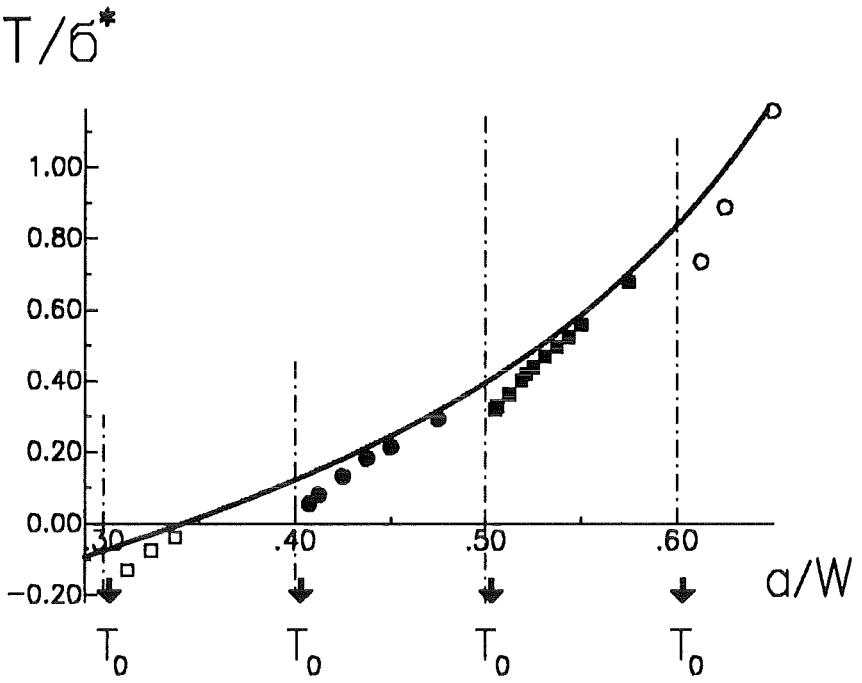

Figure 25. Bending load. T-stress term for a small crack ahead of a slender notch in bending, computed with the Boundary Collocation method for $R/W = 0.025$. Solid line: long-crack solution.

(M = bending moment, B = thickness of the component). Additionally, the "long crack solution" is introduced as solid curve. This curve represents the stress intensity factor T^* for an edge crack of total length $a = a_0 + \ell$ in bending [9]

$$T^*/\sigma^* = -4\,\frac{0.13149 - 0.6203\alpha + 0.88823\alpha^2 - 0.65955\alpha^3 + 0.2319\alpha^4}{(1-\alpha)^2} \tag{77}$$

In case of pure tension with $\sigma^* = \sigma_0$ (σ_0 = remote tensile stress) it holds [9]

$$T^*/\sigma^* = -4\,\frac{0.13149 - 0.16024\alpha - 0.051233\alpha^2 - 0.18874\alpha^3 + 0.19936\alpha^4 - 0.04915\alpha^5}{(1-\alpha)^2} \tag{78}$$

The results obtained under tension are plotted in fig.26. For the limit case $\ell/R \to 0$ the T-stress can be determined from the solution for a small crack in a plate with a tensile stress identical with the maximum normal stress σ_{max} occurring directly at the notch root

$$\sigma_{max} = 2\sigma^* F(a_0)\sqrt{\frac{a_0}{R}} \tag{79}$$

Then it holds

$$T_0 = T_{\ell/R \to 0} = \frac{T_{plate}}{\sigma^*}\bigg|_{\alpha \to 0} \sigma_{max} \tag{80}$$

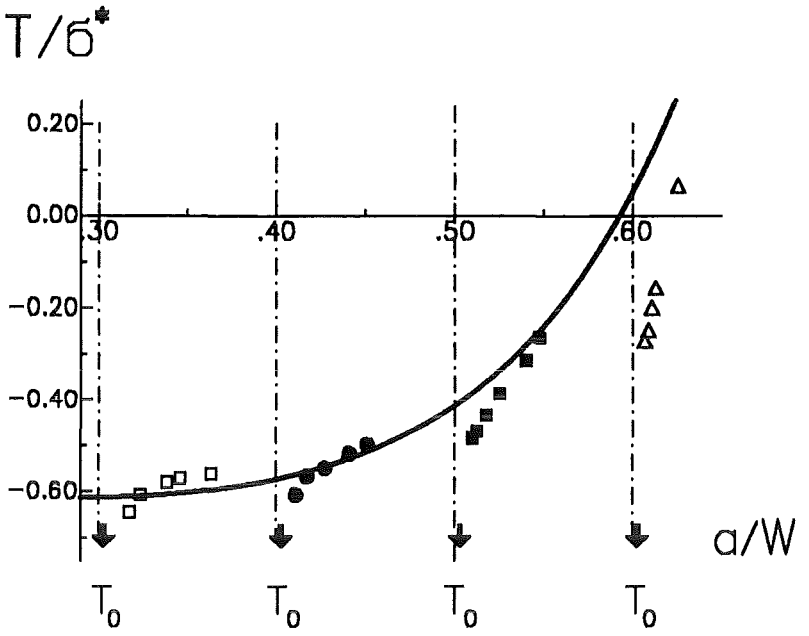

Figure 26. Tensile loading. T-stress for a small crack ahead of a slender notch under tension, computed with the Boundary Collocation method for $R/W = 0.025$. Solid line: long-crack solution.

$$T_{plate}/\sigma^* \Big|_{\alpha \to 0} = -4\left(A_0^*\right)_{plate,\,\alpha \to 0} = -0.526 \tag{81}$$

and, consequently,

$$T_0/\sigma^* = -1.052F(a_0)\sqrt{\frac{a_0}{R}} \tag{82}$$

It becomes obvious from eq.(82) that for slender notches very strong compressive T-stresses occur in the limit case $\ell/R \to 0$. The limit values T_0 for tension and bending, indicated by the arrows in figs.25 and 26, are entered in table 1.
In fig.27 both the bending and the tension results are plotted in a normalised representation. From the insert in fig.27 we can conclude that the deviation between the T-stress term for the crack/notch configuration and the long-crack solution (with the crack assumed to have a total length $a_0 + \ell$) is negligible for $\ell/R > 1$. The drastic decrease in T for $\ell/R \to 0$ must occur within the range $0 < \ell/R < 0.2$.

a/W	T_0/σ^* (bending)	T_0/σ^* (tension)
0.3	-4.11	-6.05
0.4	-5.28	-8.91
0.5	-7.01	-13.31
0.6	-9.86	-20.74

Table 4. . Limit values for the T-stress term ($\ell/R \to 0$).

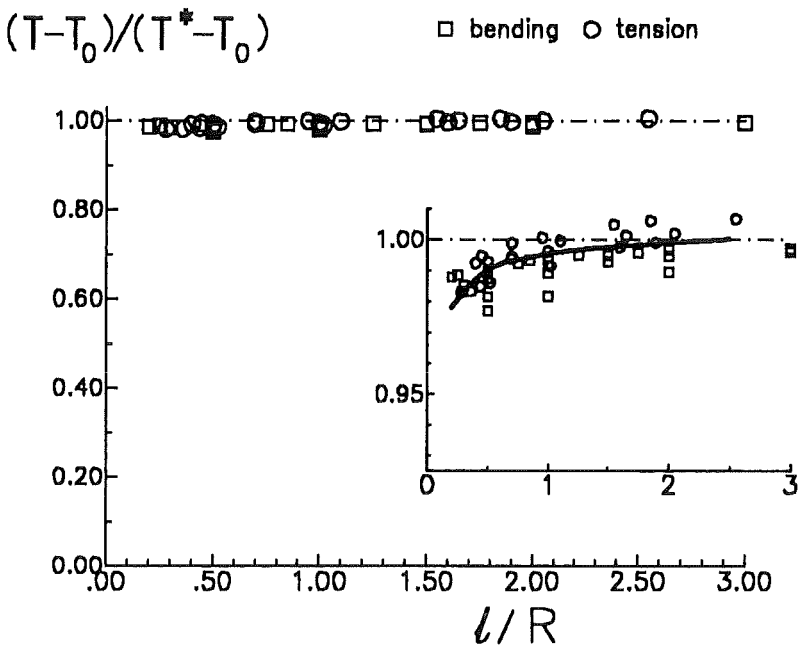

Figure 27. Circular notch. T-stress in a normalised representation.

8. Array of deep edge cracks

Figure 28 shows an array of periodical edge cracks. BCM-computations were performed for an element of periodicity for the special case of a constant remote tensile stress σ. The boundary conditions are given by constant displacements v and disappearing shear stresses along the symmetry lines, i.e.

$$v = \frac{\sigma}{E'}\frac{d}{2} \quad ; \quad \tau_{xy} = 0 \text{ for } y = \pm d/2 \tag{83}$$

($E' = E$ for plane stress and $E' = E/(1-\nu^2)$ for plane strain, E = Young's modulus, ν = Poisson's ratio) as illustrated in fig.29. The coefficient A_0^* is shown in fig.10 as a function of the ratio d/a for different relative crack lengths $\alpha = a/W$. The result can be summarised as

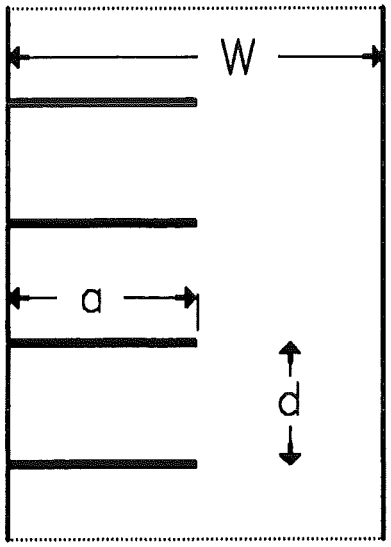

Figure 28. Crack array. Periodical edge cracks in an endless strip

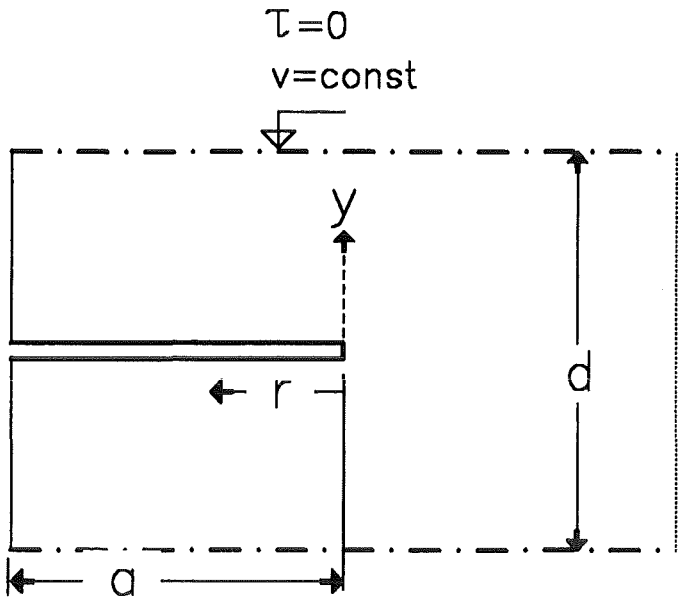

Figure 29. Periodical boundary conditions. Boundary conditions representing an endless strip with periodical cracks.

$$A_0^* = 0.148 \qquad d/a \leq 1.5 \tag{84}$$

The coefficient A_0 is plotted in fig.9 in the normalised form

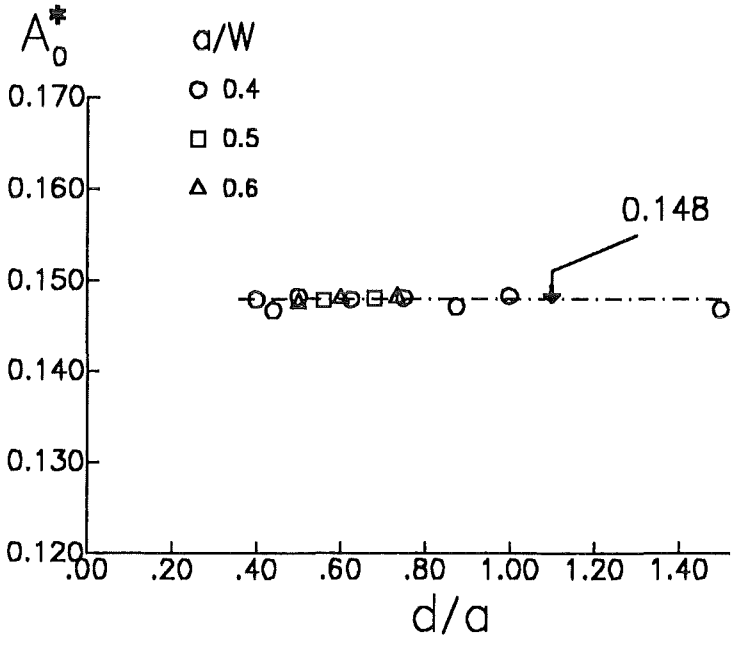

Figure 30. A_0^*. Influence of the geometric data on the coefficient A_0^* for remote tension.

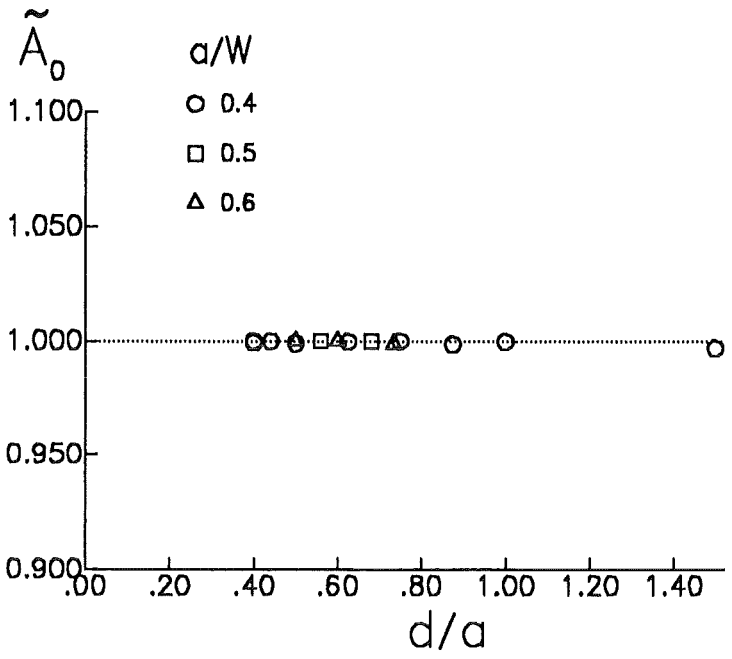

Figure 31. A_0. Coefficient A_0 in the normalisation $\tilde{A}_0 = 6A_0\sqrt{\pi W/d}$ as a function of geometry.

$$\tilde{A}_0 = 6A_0\sqrt{\pi W/d} \tag{85}$$

For all values $\alpha = a/W$ investigated it was found

$$\tilde{A}_0 = 1.000 \pm 0.002 \tag{86}$$

resulting in the stress intensity factor solution

$$K_I = \sigma\sqrt{d/2} \tag{87}$$

(see e.g. [20]). The biaxiality ratio is

$$\beta \simeq -1.484\sqrt{a/d} \tag{88}$$

9. References

[1] S.G. Larsson, A.J. Carlsson, J. of Mech. and Phys. of Solids **21**(1973),263-277.
[2] J.D. Sumpter, Int. J. Press. Ves. and Piping **10**(1982),169-180.
[3] B. Cotterell, Q.F. Li, D.Z. Zhang, Y.W. Mai, Eng. Fract. Mech. **21**(1985),239-244.
[4] P.S. Leevers, J.C. Radon, Inherent stress biaxiality in various fracture specimen geometries, Int. J. Fract. **19**(1982),311-325.
[5] A.P. Kfouri, Int. J. Fract. **30**(1986),301-315.
[6] T.L. Sham, Int. J. Solids and Struct. **25**(1989),357-380.
[7] T.L. Sham, Int. J. Fract. **48**(1991),81-102.
[8] T. Fett, A Green's function for T-stresses in an edge-cracked rectangular plate, submitted to Engng. Fract. Mech.
[9] T. Fett, D. Munz, Advances in stress intensity factors and weight functions, Computational Mechanics International, Southampton, 1996.
[10] Y.Y. Wang, D.M. Parks, Int. J. Fract. **56**(1992),25-40.
[11] M.L. Williams, On the stress distribution at the base of a stationary crack, J. Appl. Mech. **24**(1957) 109-114.
[12] G.R. Irwin, Analysis of stresses and strains near the end of a crack transversing a plate, Trans. Amer. Soc. Mech. Engnrs., J. Appl. Mechanics **24**(1957) 361-364.
[13] J. Rödel, J.F. Kelly, B.R. Lawn, In situ measurements of bridge crack interfaces in the scanning electron microscope, J. Amer. Ceram. Soc. **73**(1990) 3313-3318.
[14] G.A. Schneider, F. Magerl, I. Hahn, G. Petzow, In situ observations of unstable and stable crack propagation and R-curve behavior in thermally loaded disks, in: G.A. Schneider, G. Petzow (eds.), Thermal Shock and Thermal Fatigue Behavior of Advanced Ceramics, 229-244, 1993 Kluwer Academic Publishers, Dordrecht, Netherlands.
[15] H.-A. Bahr, T. Fett, I. Hahn, D. Munz, I. Pflugbeil, Fracture mechanics treatment of thermal shock and the effect of bridging stresses, in: G.A. Schneider, G. Petzow (eds.), Thermal Shock and Thermal Fatigue Behavior of Advanced Ceramics, 105-117, 1993 Kluwer Academic Publishers, Dordrecht, Netherlands.
[16] L.A. Wigglesworth, Stress distribution in a notched plate, Mathematica **4**(1957) 76-96.
[17] H. Bueckner, A novel principle for the computation of stress intensity factors, ZAMM **50**(1970) 529-546.
[18] S.P. Timoshenko, J.N. Goodier, Theory of Elasticity, McGraw-Hill, London, 1970.
[19] M. Creager, P.C. Paris, Elastic field equations for blunt cracks with reference to stress corrosion cracking, Int. J. Fract. **3**(1967) 247-52.
[20] H. Tada, P.C. Paris, G.R. Irwin, The stress analysis of cracks handbook, Del Research Corporation, 1986.